Synthesis of nitrogen rich (2D- 1D) hybrid carbon nanomaterial using MnO_2 nanorods template for high performance Li-ion battery application

B. P. Vinayan, Nele I. Schwarzburger and Maximilian Fichtner *

Helmholtz Institute Ulm for Electrochemical Storage (HIU), Helmholtzstr. 11,

D-89081 Ulm, Germany

Phone: +49 (0)731 50 34201, Fax: +49 (0)731 50 34299

maximilian.fichtner@kit.edu

Abstract

A novel strategy is developed to synthesis nitrogen rich (few layer graphene-carbon nanotube) [N-(FLG-CN)] hybrid material with the help of self-degradable MnO_2 nanorod templates for the application of high performance and long cyclic stability anode electrode in Li ion batteries. During the synthesis procedure, the surfaces of MnO_2 nanorods and few layer graphene (FLG) are non-covalently functionalized with a anionic and cationic polyelectrolytes, respectively for proper mixing of the constituents. Polymerization of this one and two dimensional hybrid composite with a nitrogen containing polymer and subsequent pyrolysis at 800 °C temperture lead to the formation of highly porous nitrogen doped-(FLG-CN) hybrid nanocomposite with a nitrogen doping level of 9.3 wt. %. The N-(FLG-CN) electrode material in Li ion batteries displays superior reversible capacities of 739 mAh g^{-1} after 30^{th} cycle at the current density of 100 mA g^{-1} and 445 mAh g^{-1} after 500^{th} cycle at the high current density of 500 mA g^{-1}. As compared to pristine graphene material, N doped (FLG-CN) hybrid material shows two times enhancement in specific capacity at high current densities (~ 5000 mA g^{-1}) and long cyclic stability (1000 cycles). The highly defective and porous 1D-2D morphology of N-(FLG-CN) hybrid structure gives more adsorption sites for lithium ions, meanwhile nitrogen doping significantly reduces the charge transfer resistance of graphene based electrodes.

Key words: Nitrogen doping, Few layer graphene, Carbon nanotube, Non-covalent functionalization, MnO_2 nanorod, Lithium ion battery.

Introduction

The limited supply of fossil fuels and necessity of low carbon economy in the modern world have increased the demand for electric vehicles (EV) and the main power source for these vehicles are rechargeable lithium ion batteries (LIBs). The major technological challenge is the development of battery electrode materials simultaneously with superior power and high energy capacity at fast charge-discharge rates. The present LIBs with graphite as anode electrode (theoretical capacity ~ 372 mAh g^{-1}) are insufficient to meet the requirement of high energy and power densities of these EV. At the same time, anode electrode materials like SnO_2, Si, Sn and different transition metal oxides (Co_3O_4, Fe_2O_3, NiO etc.) exhibit large voltage hysteresis between charge and discharge and poor cyclic performance arising from the huge volume expansion during lithium insertion/extraction.[1-3] In this aspect, carbon nanomaterials are very promising because of their high capacity as compared to graphite and long cyclic stability.[4]

Recently, different kinds of carbon nanomaterials have been studied for LIB application such as carbon nanotubes (CNTs), carbon nanofibres (CNFs), nanocoils, graphite nanoplatelets, few layer graphene, and various mesoporous carbons.[2, 4-6] Among these carbon nanomaterials, graphene (G) based nanostructures have emerged as preferred materials for energy storage applications due to their unique properties such as large surface area, high charge mobility, excellent electronic and thermal conductivity, high mechanical strength and good chemical stability.[7] Theoretical calculations show that Li can be adsorbed on both faces of a single layer graphene with the formation of Li_2C_6 intercalation compound and hence a theoretical capacity of 744 mAh g^{-1}.[8, 9] However, the capacity loss for graphene samples as synthesized from graphite oxide is quite high during cycling.[10, 11] This is mainly due to the presence of higher amount of oxygen functional groups and considerable agglomeration of

sheets within the graphene structures, which lead to large irreversible capacity, low electronic conductivity and decrease in Li adsorption sites.

To increase the specific capacity and stability of graphene based anode materials, new approaches should include (a) proper chemical modifications of graphene surfaces without destructing their novel properties and (b) the incorporation of conductive spacers in between graphene sheets to prevent their restacking. Among different kinds of surface chemical modifications techniques of graphene, nitrogen (N) doping is promising technique especially for LIB applications because it can promote better electrochemical performances and increased electronic conductivity to the pristine graphene.[1, 12] For example, Zhong-Shuai et al. reported that reversible capacity of LIB could increase from 66.8 % for the pristine graphene electrode to 83.6 % for the N-doped graphene electrode with a nitrogen doping amount of 3.06 %.[12] In another report, Wang et al. showed that Li storage capacity can improve by 2 % nitrogen doping level up to 900 mAh g^{-1} at a current density of 42 mA g^{-1}, which is higher than that of pure graphene.[13] In the case of incorporation of conductive spacers in between graphene sheets, CNTs, fullerenes, and metal/metal oxide nanoparticles etc are promising candidates.[2, 11, 14] It has been reported that the incorporation of MWNTs along with graphene sheets avoids the restacking of graphene sheets and also enhances the electrical conductivity of the nanocomposite and gives improved electrochemical performances in LIB applications.[15, 16]

In this work, we developed a novel approach for the synthesis of nitrogen doped (few layer graphene - carbon nanotubes) hybrid nanomaterial using MnO_2 nanorods as self degradable template and subsequently investigated its electrochemical properties as anode electrode in Li ion battery. The study shows that this highly porous, large surface area and nitrogen rich hybrid nanostructure of one and two dimensional morphology can deliver high specific capacity, superior rate capability with less charge transfer resistance and long cyclic stability.

2. Experimental Details

2.1. Synthesis of materials

Few layer graphene (FLG) was synthesized by the thermal exfoliation of graphite oxide (GO) at 1050 °C in Argon atmosphere.[17, 18] MnO_2 nanorods (MN) were prepared by hydrothermal synthesis method, which is explained elsewhere.[19] The pristine FLG was functionalized by a cationic polyelectrolyte poly-(diallyldimethyl ammonium chloride) (PDDA, 20 wt. % in water) to attach positive surface functional groups,[20] and the sample was labeled as PDDA-FLG. During this procedure, 300 mg of FLG was initially dispersed in 1200 mL of de-ionized (DI) water by ultrasonication in the presence of 0.5 wt. % PDDA and 0.5 wt. % NaCl. The final solution was then filtrated and washed several times to remove the excess PDDA and subsequently dried in vacuum at 60 ◦C for 24 h.

Pristine MnO_2 nanorods were surface functionalized with an anionic polyelectrolyte poly (sodium 4-styrenesulfonate) (PSS, Mw ~ 70,000, 30 wt. % in H_2O) to attach negative surface functional groups. For this, 200 mg of MnO_2 nanorods were dispersed in 1 wt. % aqueous solution of PSS by ultrasonication, and then the suspension was stored at 65 °C for 12 h. The final samples were filtered and washed with de-ionized (DI) water to remove the excess polyelectrolytes and dried at 60 °C in vacuum for 12 h. After functionalization of MnO_2 nanorods, the sample was labeled as PSS-MN.

PDDA-FLG (200 mg) and PSS-MN (200 mg) were mixed together in the weight ratio (1:1) by ultrasonication followed by stirring for 8 h in DI water medium. Subsequently, (PDDA-FLG + PSS-MN) hybrid structure was coated with nitrogen containing polymer, polypyrrole (PPy) using the monomer pyrrole (250 µL) and ammonium persulfate (25 mL) in an acidic medium of 0.1 M HCl (200 mL). The final solution was stirred for 24 h at room temperature.

Then filtered and washed repeatedly with DI water and ethanol and dried at 60 °C for 12 h. PPy coated hybrid structure was further pyrolized at 800 ºC in argon gas atmosphere to form nitrogen rich (graphene-carbon nanotube) [N-(FLG-CN)] hybrid structure.

2.2. Characterization techniques

The vibrational properties of the samples were investigated by Raman spectroscopy and Fourier transform infrared spectroscopy (FTIR). Raman measurements were taken in the spectral range of 1000–3500 cm^{-1} using a confocal InVia, Raman micro spectrometer with a 532 nm laser (RENISHAW) as the excitation source. FTIR experiments were carried out in the spectral range of 500-4000 cm^{-1} using a PerkinElmer's FTIR spectrometer. X-ray photoelectron spectroscopy (XPS, SPECS GmbH spectrometer) was carried out to find out the oxidation state and amount of nitrogen present in the samples. The X-ray diffraction (XRD) measurements were carried out in a Stadi P diffractometer (STOE & Cie GMBH) with a MYTHEN detector using Cu K_α radiation as the X-ray source. The morphological studies of the samples were studied by scanning electron microscope (SEM, LEO GEMINI 1550 VP) and transmission electron microscope (TEM). Energy dispersive spectroscopy (EDS) was carried out in SEM equipped with Silicon Drift Detector (OXFORD Instruments). Thermo gravimetric analysis (TGA) of the sample was recorded with a Mettler Toledo TGA/sDTA 851e instrument from ambient temperature to 900 ºC in an air atmosphere with a heating rate of 20 ºC min^{-1}. Brunauer-Emmett-Teller (BET) surface area analyses of the samples were carried out with a Micromeritics ASAP 2020 MP system.

2.3. Electrochemical measurements

The battery electrodes were constructed by mixing 90 wt. % of active material with 10 wt. % polyvinylidenefluoride (PVDF) binder using N-methyl-2-pyrrolidinone as solvent. The slurry

was uniformly coated over a stainless steel current collector (10 mm) and dried at 100 °C in vacuum oven for 12 h to remove the solvent. Electrochemical measurements have been carried out using a Swagelok type two-electrode cell with lithium metal as the counter/reference electrode, glass microfiber filter as the separator, and 1 M $LiPF_6$ dissolved in a mixture of ethylene carbonate (EC) and dimethyl carbonate (DMC) (EC/DMC, 1 : 1 v/v) as the electrolyte. The whole assembling of the cells was carried out in an Argon filled glovebox (MBraun, Germany) equipped with recirculation and purification system to keep the water and oxygen content below 0.1 ppm. Galvanostatic charge-discharge experiments were conducted using a electrochemical workstation (ARBIN INSTRUMENTS) between 3 and 0.01 V vs. Li^+/Li at room temperature and specific capacities were calculated based on the mass of active material. Cyclic voltammetry (CV) experiments for the cells have been carried out from 0.01 to 3 V at a scan rate of 0.05 mV s^{-1} using Bio-Logic VMP-3 potentiostat. The ac impedance analyses of the cells were done by applying a sine wave with amplitude of 5.0 mV over the frequency range from 100 kHz to 0.01 Hz using Bio- Logic electrochemical work station.

3. Results and Discussion

Nitrogen rich (few layer graphene-carbon nanotube) hybrid nanostructure [N-(FLG-CN)] was successfully synthesized by using self degradable MnO_2 nanorods and few layer graphene as the starting materials as shown in synthesis scheme Fig. 1. Fig. 2(a-b) depicts the SEM and TEM images of the MnO_2 nanorods and FLG. The SEM and TEM images show that the surfaces of as synthesized MnO_2 nanorods were very smooth. The diameter of the MnO_2 nanorods was in the range of 25 to 75 nm and the length was approximately 2 to 3 μm. Electron microscope images of the FLG (Fig. 2(c-d)) show that graphene sheets were homogeneously exfoliated by thermal reduction of graphite oxide. The sheets were highly

porous and wrinkled in morphology. FTIR spectrum shows the presence of different oxygen containing functional groups such as hydroxyl, epoxyl and carbonyl, within FLG even after thermal reduction (Fig. S1: Supporting information).

The PDDA functionalization induces positive surface charges on graphene and PSS functionalization creates negative surface charges on MnO_2 nanorods as illustrated in Fig.1.[21, 22] The mixing of these surface functionalized 1 D and 2 D morphologies by ultrasonication and subsequent stirring gives a highly dispersive solution of FLG and MN in DI water. The N^+ groups of PDDA present over the surface of FLG and SO_3^- groups of PSS over the surface MN induce a electrostatic attraction between these morphologies and which promote the formation of sandwich layered structures as shown in Fig.1.[22] Here MnO_2 nanorods play the role of spacers between the graphene sheets and prevent the self-agglomeration of sheets within the solution.

During the polymerization of pyrrole monomer over the surface of (PDDA-FLG + PSS-MN) hybrid structure, the MnO_2 nanorods itself work as oxidant and templates for the formation of polypyrrole nanotubes. In acidic environment, MnO_2 acts as a strong oxidant with the following reactions,[23, 24]

$MnO_2 + 4H^+ + 2e^- \rightarrow Mn^{2+} + 2H_2O$ ($E° = 1.23$ V)

Since the oxidation potential of pyrrole (0.8V) is lower than that of MnO_2 oxidation potential (1.23 V), MnO_2 is capable of oxidizing the pyrrole monomer and subsequent formation of polypyrrole in the acidic environment.[25]. During the polymerization of pyrrole, MnO_2 becomes Mn^{2+} and which gradually dissolves in the solution.[26]

Subsequent pyrolysis of this polypyrrole (1D-2D) hybrid structure at high temperature (800 °C) leads to the decomposition of PPy and formation of nitrogen rich (graphene-carbon nanotube) hybrid structure. The SEM and TEM images (Fig. 2 (e,f)) confirm the formation of this 1D-2D hybrid structure, where carbon nanotubes act as conductive spacers in between graphene sheets. The inset image of Fig.2 (f) confirms the complete removal of MnO_2 nanorods during the formation of nitrogen rich carbon nanotubes (N-CN). For N-CN, the inner tube diameter is about ~ 75 nm and outer tube diameter is ~ 170 nm.

Fig.3 depicts the powder X-ray diffractograms of (a) graphite oxide (b) few layer graphene, (c) MnO_2 nanorods, (d) (PDDA-FLG + PSS-MN) hybrid structure, and (e) N doped (FLG-CN) hybrid nanocomposite, respectively. It has been observed from the XRD of GO (Fig.3 (a)) that upon oxidation, the intense crystalline peak of graphite at (002) plane is shifted to smaller angles (2θ=10.54°). This indicates an increase in the interlayer spacing of GO to 0.84 nm, mainly due to the intercalation of oxygen containing functional groups in between the graphene layers.[10, 18] After thermal exfoliation of GO, the 10.54° peak vanishes and a broad peak ranging from 15° to 30° appears ((Fig.3 (b))). This broad peak is an indication of loss of long range order in the few layered structure of graphene. The interlayer spacing shrinks to 0.37 nm in that case, which hints at the removal of oxygen containing functional groups from the layers during thermal exfoliation.[27] XRD of MnO_2 nanorods (Fig.3 (c)) shows that MnO_2 has been crystallized in the tetragonal phase of α-MnO_2, (JCPDS, 44-0141), and also any impurity peaks are not observed in the spectrum.[28] (PDDA-FLG + PSS-MN) hybrid structure (Fig. 3(d)) gives the broad (002) XRD peak of FLG and the peaks corresponding to the tetragonal phase of α-MnO_2. In the XRD of N-(FLG-CN) hybrid structure, the MnO_2 reflections have disappeared as shown in Fig.3 (e), which suggests the removal of MnO_2 nanorod templates after the polymerization with pyrrole. The hybrid structure shows a broad

peak at around the 2θ value of 26°, which indicates the amorphous nature of N-doped (FLG-CN) hybrid structure with small degree of graphitization.

Raman spectrum of FLG and [N-(FLG-CN)] hybrid structure is shown in Fig. 4. Two prominent peaks have been observed in the Raman spectrum of FLG at 1362 cm^{-1} and 1605 cm^{-1}, which correspond to D and G band, respectively. The D and G bands for [N-(FLG-CN)] hybrid structure are at the positions of 1349 cm^{-1} and 1596 cm^{-1}, respectively. The G band is in connection with the E_{2g} mode of phonon vibrations of sp^2-bonded carbon materials and D band arises mainly due to the large number of defects present in the carbon samples.[29] Raman spectrum of [N-(FLG-CN)] hybrid structure also shows a prominent 2D and 2D′ bands at the positions of 2672 cm^{-1} and 2941 cm^{-1}, respectively and these bands are the overtone of D band.[30] The intensity ratio between G band and D bands (I_D/I_G) is an indirect measure of the degree of defects present in the graphene based samples. The I_D/I_G ratio for the samples FLG and [N-(FLG-CN)] hybrid structure is 0.78 and 1.22, respectively, which indicates that nitrogen doping induces lot of defects within the hybrid structure and promotes a high intensity D band. Compared to that of pristine FLG, the Raman spectrum of N doped graphene hybrid nanocomposite shows a downshift for G-band (11 cm^{-1}) and D band (13 cm^{-1}) and this downshifts suggest that N dopants move the Fermi level in the upward direction.[31]

Fig. 5 represents the TGA curve of PSS-MN and [N-(FLG-CN)] hybrid structure in the air atmosphere. The small weight loss (less than 5 wt. %) for PSS-MN within 500 °C temperature is mainly due to the loss of water and decomposition of PSS polyelectrolyte. For [N-(FLG-CN)] hybrid structure, it has been observed that a complete decomposition of the sample at 600 °C due to the oxidation of carbon, which is also a direct proof for the complete degradation of MnO_2 nanorods during the polymerization process.

The pore texture properties of the [N-(FLG-CN)] hybrid structure were evaluated by nitrogen adsorption and desorption measurements and the results are illustrated in Fig. 6. The sample displays a type IV isotherm with a small hysteresis loop (Fig. 6(a)), indicating the micro porous structure.[32, 33] The BET surface area, average pore volume and pore diameter of the N-(FLG-CN)] sample were 962 m^2 g^{-1}, 1.23 cm^3 g^{-1} and 4.65 nm, respectively. The pore size distribution (PSD) plot (Fig. 5(b)) shows that mainly micro pores (< 5 nm) are present in the sample and in addition small amount of macro pores (> 50 nm) also. The relatively high specific area of the N-(FLG-CN) hybrid structure (~ 962 m^2 g^{-1}) as compared to FLG (~ 456 m^2 g^{-1} - Fig.S2: Supporting Information) is ascribed to abundant micro pores. Meanwhile the presence of wide range of macropores distribution permits the efficient transportation and permeability of electrolytes through the electrode materials.

The high resolution N1s XPS spectrum of nitrogen doped (FLG-CN) hybrid structure is shown as Fig.7. The deconvolution of N1s spectrum reveals the existence of three different oxidation states for nitrogen, such as pyridinic, pyrrolic and graphitic N at the binding energies of 393.45 eV, 394.75 eV and 397.13 eV, respectively.[1] Here, pyridinic-N corresponds to nitrogen atoms at the edge of graphene planes and bonded to two carbon atoms, thus donating one *p* electron to the aromatic π system. Pyrrolic-N atoms are bonded to two carbon atoms and contribute two *p* electrons to aromatic π system.[34] Graphitic (quaternary) nitrogen atoms simply substitute the carbon atoms within the graphene lattice. The total amount of nitrogen contained in the hybrid structure was calculated from the peak areas of the XPS spectrum and which gave a value of 9.2 atomic %. The relative contribution of pyridinic N, pyrrolic N and graphitic N to the total amount of doped N was 23.37 %, 47.26 % and 29.37 %, respectively, which shows that major contribution are coming from the pyrrolic type N atoms.

Fig. 8 shows the EDS spectrum of nitrogen doped (FLG-CN) sample and that gives the weight percentage of different elements present in the sample such as carbon (84.3 %), nitrogen (9.3 %) and oxygen (6.4 %). The absence of Mn peaks in the EDS spectrum is another confirmation of the removal of MnO_2 nanorod template during the polymerization process. Fig. 8 also depicts the elemental mapping of carbon, nitrogen and oxygen, which shows the uniform distribution of doped N atoms throughout the sample.

Electrochemical study

The galvanostatic charge-discharge profiles have been shown in Fig. 9 (a) and Fig. 10 (a) for nitrogen doped (FLG-CN) hybrid nanocomposite and few layer graphene (FLG) electrode materials at a current density of 100 mA g^{-1}. N-(FLG-CN) electrode gave an initial discharge (lithiation) capacity of 1106 mAh g^{-1} and a charge (delithiation) capacity of 934 mAh g^{-1} (See Table 1). The cyclic voltammetry (CV) of N-(FLG-CN) electrode for the first cycle at a scan rate of 0.05 mV s^{-1} has been given in Fig.S4 (See supporting information for details). During the 2^{nd}, 3^{rd} and 4^{th} battery cycles, the discharge capacities were reduced to 904, 816, 793 mAh g^{-1}, respectively and become almost stable. At the end of 30^{th} cycle, the discharge and charge capacities were 739 and 736 mAh g^{-1}, respectively. The corresponding coulombic efficiencies for the 1^{st} and 30^{th} cycles were ~ 85 % and ~ 100 %. N-(FLG-CN) electrode retained 82 %, and 67 % of its first discharge capacity after 2^{nd} and 30^{th} cycles, respectively. At the same time, FLG delivered a first discharge and charge capacity of 1611 mAh g^{-1} and 1068 mAh g^{-1}, respectively, with a coulombic efficiency of 66.3 %. The discharge capacities were further decreased to 800, 657, 450 mAh g^{-1}, respectively after 2^{nd}, 3^{rd} and 30^{th} cycles with the coulombic efficiencies of 85 %, 89 % and 98.8 %. FLG electrode could deliver only 49.7 %, and 27.9 % of its initial capacity after 2^{nd} and 30^{th} cycles, respectively. During the first discharge of electrode materials, the voltage plateau above 0.6 V is mainly coming from the

electrolyte decomposition, formation of solid electrolyte interface (SEI) and the reduction of oxygen functional groups present in the electrode materials.[17, 35] The width of this plateau is small in N-(FLG-CN) as compared to FLG and hence low irreversible capacity also observes in this electrode material. This is mainly due to presence of less oxygen functional groups and rich nitrogen contents present in N-(FLG-CN) electrode, which has been already verified by XPS (Fig.7 and Fig. S1: Supporting information) and EDX (Fig.8). One recent report shows that N or B doping can reduce the electrolyte decomposition and surface side reactions between graphene electrode and electrolyte to form an SEI film.[12] Further charge-discharge profiles of the N-(FLG-CN) and FLG electrode materials resemble that of conventional hard carbons due to the presence of their disordered structures, high porosity, presence of hetero atoms and dangling bonds.[4] In these electrode materials, above 0.5 V the Li storage is mainly taking places at the defect sites, micropores, surfaces and hence the capacity contribution is directly proportional to the specific surface area of electrode materials.[17, 36] Below 0.5 V, the capacity contribution is attributed to the intercalation of lithium into the graphene or nanotube layers.[36]

The most important aspect of N doped (FLG-CN) electrode materials is their superior charge and discharge performances in LIBs at high current densities. Fig. 9 (b) and Fig. 10 (b) show the charge-discharge profiles of the N-(FLG-CN) and FLG electrode materials at different high current densities after running the cell for the initial 30 cycles at the current density of 100 mA g^{-1}. Table 1 compares the values of discharge capacities for FLG and N-(FLG-CN) electrode materials at the current densities of 100, 500, 1000, 2500 and 5000 mA g^{-1}, respectively. The current rate capabilities of N-(FLG-CN) at other current densities are shown in Fig. S3 (Supporting Information). These results show that current rate capability of N doped (FLG-CN) electrode material is far improved as compared to pristine graphene and previously reported anode materials such as graphite,[37] graphene nanosheets,[38, 39], nitrogen

doped graphene nanosheets,[13] carbon nanotubes,[6, 35] and carbon nanobeads.[5] It has been observed that N doped (FLG-CN) electrode gives more capacity contribution above 0.5 V (lithium adsorption on defects, edges and micropores) than those below 0.5 V (lithium intercalation) at high current densities. Meanwhile for FLG, the capacity contribution below 0.5 V at high current densities is higher or equal to those above 0.5 V. These results imply that N doping and 1D -2D morphology of the hybrid structure plays an important role for increasing the defects and faradic capacitance within the N-(FLG-CN) electrode material.

The cycling stability of the N doped (FLG-CN) anode materials was further tested by running a fresh cell initially for 500 cycles at the current density of 500 mA g^{-1}, and after that the same cell was cycled again for the next 500 cycles at the high current density 5000 mA g^{-1}, as shows in Fig. 11. The discharge capacity of the cell was 630 and 541 mAh g^{-1}, for the first and second cycles, respectively (Figure 11 (a)) at the current density of 500 mA g^{-1}. At the end of 500^{th} cycle, the discharge capacity was decreased to 445 mAh g^{-1} with 83 % retention capacity of its second cycle. During the next 500 cycles of the same cell with the high current density of 5000 mA g^{-1} (Figure 11 (b)), the initial discharge capacity was 212 mAh g^{-1}. After 500 cycles, the discharge capacity was reduced to 205 mAh g^{-1}, with 97 % retention capacity of the initial cycle and almost 100 % coulombic efficiency also.

To get more information about the electrochemical performance of N-(FLG-CN) and FLG electrode materials, ac impedance experiments were carried out for the cell in a charged state (3.0 V vs. Li^+/Li) after running an initial 5 cycles. The Nyquist plot and matching equivalent electrical circuit are depicted in Figure 12. In the Nyquist plot, the high frequency semicircle is associated with the lithium-ion migration through the SEI film formed over the carbon nanomaterials, middle frequency semicircle is connected to the charge transfer through the electrode/electrolyte interface and the steep sloping line represents solid-state diffusion of the lithium-ion in the electrode.[13] In the equivalent electrical circuit model, R_E is the resistance of

the electrolyte and separator; it is 6.3 Ω and 7.4 Ω, respectively for the N-(FLG-CN) and FLG electrode materials. R_{SEI} and $CPE_{SEI,}$ are the resistance and constant phase element of the SEI formed on the electrode. For the N-(FLG-CN) and FLG electrode materials the R_{SEI} values were 23.7 Ω and 49.9 Ω respectively, which shows the formation of a thin SEI layer over the surface of N-(FLG-CN) anode material as compared to FLG that promotes an easy lithium ion transfer at the interface between the electrolyte and the electrode. R_{CT} is the charge transfer resistance and Z_w is the Warburg impedance related to the diffusion of lithium ions into the bulk electrode.[40] The charge transfer resistances (R_{CT}) were 11.5 Ω and 34.6 Ω for the electrode materials N-(FLG-CN) and FLG, respectively, which indicates the high electronic and Li ionic conductivity within the N-(FLG-CN) anode electrode.

The higher performance of nitrogen doped (FLG-CN) hybrid anode material achieved in the present work is mainly due to the following reasons. First, the 1D-2D special morphology of the hybrid structure provide more storage sites for lithium ions due to their large surface areas, high porosity and pore volume. Here the one dimensional carbon nanotube structures act as conductive spacers in between 2 dimensional graphene layers and that prevent the restacking of sheets usually observed in pristine graphene based anode materials, which help for the formation of Li_2C_6 rather than LiC_6 structures as shown in the schematic Fig.13.[11, 41] 2D graphene sheets endorse faster lithium ion diffusion on the surface and highly conductive of carbon nanotubes decreases the resistance that ions experience in moving from one graphene layer to the other.[10] Another contribution to the high performance of N-(FLG-CN) anode material is mainly coming from the nitrogen doping effects. Pyridinic and pyrrolic nitrogen can contribute addition electron charge density over the surface of graphene layers that reduces the energy barrier for Li ion penetration and increases electrical conductivity which results in a high reversible capacity at high current densities.[42] In addition, N doping can create topological defects over the surfaces of hybrid structures that enhance the capacity.

It has been already observed that N doping can reduce the electrolyte decomposition and promotes higher electrode/electrolyte wettability, which increases the reversible capacity and faster lithium ion diffusion to the interface and bulk of electrode material.[12] All these characteristics of N doped (FLG-CN) material make them a suitable anode electrode material for high power applications with high capacity, superior rate capability and long cyclic stability.

Conclusion

In summary, high yield nitrogen rich (few layer graphene-carbon nanotube) hybrid structure electrode material, a unique combination of 2D and 1D structures, has been synthesized using graphene sheets and MnO_2 nanorod self degradable template. It has been observed that the surface modifications of graphene sheets and MnO_2 nanorods using a cationic and anionic polyelectrolytes helps for the better mixing of constituents through the electrostatic attraction. N doped (FLG-CN) hybrid electrode material in LIB provides high reversible capacity, superior rate capability and long cyclic stability at high current densities due to its large surface area, more number of heteroatomic defects, reduced charge transfer resistance, and improved electrode/electrolyte wettability. The synthesis approach is facile and low cost and it can open a new pathway for the development of high power and large energy density electrochemical storage devices for powering electric vehicles.

References

1. B.P. Vinayan, and S. Ramaprabhu, *J. Mater. Chem. A*, 2013, **1**, 3865-3871.
2. Z.-S. Wu, G. Zhou, L.-C. Yin, W. Ren, F. Li and H.-M. Cheng, *Nano Energy*, 2012, **1**, 107-131.
3. S. W. Lee, M. T. McDowell, J. W. Choi and Y. Cui, *Nano Letters*, 2011, **11**, 3034-3039.
4. N. A. Kaskhedikar and J. Maier, *Advanced Materials*, 2009, **21**, 2664-2680.
5. J.-C. Chang, Y.-F. Tzeng, J.-M. Chen, H.-T. Chiu and C.-Y. Lee, *Electrochimica Acta*, 2009, **54**, 7066-7070.
6. H. C. Shin, M. Liu, B. Sadanadan and A. M. Rao, *Journal of Power Sources*, 2002, **112**, 216-221.
7. Y. Sun, Q. Wu and G. Shi, *Energy & Environmental Science*, 2011, **4**, 1113-1132.
8. M. Liu, A. Kutana, Y. Liu and B. I. Yakobson, *The Journal of Physical Chemistry Letters*, 2014, **5**, 1225-1229.
9. X. Fan, W. T. Zheng and J.-L. Kuo, *ACS Applied Materials & Interfaces*, 2012, **4**, 2432-2438.
10. B.P. Vinayan, R. Nagar and S. Ramaprabhu, *Journal of Materials Chemistry*, 2012, **22**, 25325-25334.
11. E. Yoo, J. Kim, E. Hosono, H.-s. Zhou, T. Kudo and I. Honma, *Nano Letters*, 2008, **8**, 2277-2282.
12. Z.-S. Wu, W. Ren, L. Xu, F. Li and H.-M. Cheng, *ACS Nano*, 2011, **5**, 5463-5471.
13. H. Wang, C. Zhang, Z. Liu, L. Wang, P. Han, H. Xu, K. Zhang, S. Dong, J. Yao and G. Cui, *Journal of Materials Chemistry*, 2011, **21**, 5430-5434.
14. D. Yu and L. Dai, *The Journal of Physical Chemistry Letters*, 2009, **1**, 467-470.
15. M. Sahoo, B. P. Vinayan and S. Ramaprabhu, *RSC Advances*, 2014, **4**, 26140-26148.

16. H.-J. Peng, J.-Q. Huang, M.-Q. Zhao, Q. Zhang, X.-B. Cheng, X.-Y. Liu, W.-Z. Qian and F. Wei, *Advanced Functional Materials*, 2014, **24**, 2772-2781.

17. H. F. Xiang, Z. D. Li, K. Xie, J. Z. Jiang, J. J. Chen, P. C. Lian, J. S. Wu, Y. Yu and H. H. Wang, *RSC Advances*, 2012, **2**, 6792-6799.

18. W. S. Hummers and R. E. Offeman, *J. Am. Chem. Soc.*, 1958, **80**, 1339.

19. S. Lim and J. Cho, *Electrochemistry Communications*, 2008, **10**, 1478-1481.

20. W. Shuangyin, J. San Ping and W. Xin, *Nanotechnology*, 2008, **19**, 265601.

21. B. P. Vinayan, R. Nagar, N. Rajalakshmi and S. Ramaprabhu, *Advanced Functional Materials*, 2012, **22**, 3519-3526.

22. B. Wu, C. Li, H. Yang, G. Liu and G. Zhang, *The Journal of Physical Chemistry B*, 2012, **116**, 3106-3114.

23. W. Chen, R. B. Rakhi and H. N. Alshareef, *The Journal of Physical Chemistry C*, 2013, **117**, 15009-15019.

24. W. Chen, R. B. Rakhi and H. N. Alshareef, *Journal of Materials Chemistry A*, 2013, **1**, 3315-3324.

25. R. Ansari, *E-Journal of Chemistry*, 2006, **3**, 186-201.

26. X. Feng, Y. Zhang, Z. Yan, N. Chen, Y. Ma, X. Liu, X. Yang and W. Hou, *Journal of Materials Chemistry A*, 2013, **1**, 9775-9780.

27. B.P. Vinayan, R. Nagar and S. Ramaprabhu, *J. Mater. Chem. A*, 2013, **1**, 11192-11199.

28. F. Cheng, J. Zhao, W. Song, C. Li, H. Ma, J. Chen and P. Shen, *Inorganic Chemistry*, 2006, **45**, 2038-2044.

29. S. Reich and C. Thomsen, *Philosophical Transactions of the Royal Society of London. Series A: Mathematical, Physical and Engineering Sciences*, 2004, **362**, 2271-2288.

30. A. Kaniyoor and S. Ramaprabhu, *AIP Advances*, 2012, **2**, 032183.

31. R. Lv, Q. Li, A. R. Botello-Méndez, T. Hayashi, B. Wang, A. Berkdemir, Q. Hao, A. L. Elías, R. Cruz-Silva, H. R. Gutiérrez, Y. A. Kim, H. Muramatsu, J. Zhu, M. Endo, H. Terrones, J.-C. Charlier, M. Pan and M. Terrones, *Sci. Rep.*, 2012, **2**, 586.

32. M. Khalfaoui, S. Knani, M. A. Hachicha and A. B. Lamine, *Journal of Colloid and Interface Science*, 2003, **263**, 350-356.

33. P. Schneider, *Applied Catalysis A: General*, 1995, **129**, 157-165.

34. B.P. Vinayan, R. Nagar and S. Ramaprabhu, *Langmuir*, 2012, **28**, 7826-7833.

35. E. Frackowiak, S. Gautier, H. Gaucher, S. Bonnamy and F. Beguin, *Carbon*, 1999, **37**, 61-69.

36. M. Winter, J. O. Besenhard, M. E. Spahr and P. Novák, *Advanced Materials*, 1998, **10**, 725-763.

37. C. Wang, A. J. Appleby and F. E. Little, *Journal of Electroanalytical Chemistry*, 2001, **497**, 33-46.

38. G. Wang, X. Shen, J. Yao and J. Park, *Carbon*, 2009, **47**, 2049-2053.

39. A. Abouimrane, O. C. Compton, K. Amine and S. T. Nguyen, *The Journal of Physical Chemistry C*, 2010, **114**, 12800-12804.

40. Y. Sharma, N. Sharma, G. V. Subba Rao and B. V. R. Chowdari, *Chemistry of Materials*, 2008, **20**, 6829-6839.

41. R. I. Jafri, T. Arockiados, N. Rajalakshmi and S. Ramaprabhu, *Journal of The Electrochemical Society*, 2010, **157**, B874-B879.

42. H. J. Yan, B. Xu, S. Q. Shi and C. Y. Ouyang, *Journal of Applied Physics*, 2012, **112**, -.

Tables

Table I. The discharge capacities of FLG and N-(FLG-CN) for the initial cycles and different current densities.

Current density (mA g^{-1})	**Discharge capacity of FLG (mAh g^{-1})**	**Discharge capacity of N-(FLG-CN) (mAh g^{-1})**
100	1611 (1^{st} cycle)	1106 (1^{st} cycle)
100	800 (2^{nd} cycle)	904 (2^{nd} cycle)
100	450 (30^{th} cycle)	739 (30^{th} cycle)
500	296	496
1000	228	351
2500	155	266
5000	116	215

Figure captions

Fig. 1: Schematic diagram of the synthesis procedure adopted for making the N doped (FLG-CN) hybrid nanocomposite.

Fig. 2: Scanning and transmission electron micrographs of MnO_2 nanorods (a, b), few layer graphene structure (c, d), and N doped (FLG-CN) hybrid nanocomposite (e, f). Inset in (f) depicts the magnified portion of a nanotube within the N doped (FLG-CN) hybrid structure, which clearly shows the removal of MnO_2 nanorod template.

Fig. 3: X-ray diffractograms of (a) graphite oxide (b) few layer graphene, (c) MnO_2 nanorods, (d) (PDDA-FLG + PSS-MN) hybrid structure, and (e) N doped (FLG-CN) hybrid nanocomposite.

Fig. 4: Raman spectra of N doped (FLG-CN) and few layer graphene.

Fig. 5: (a) Nitrogen adsorption and desorption isotherms and (b) differential pore volume of the N doped (FLG-CN) hybrid nanocomposite.

Fig. 6: High resolution N1S XPS spectra of N doped (FLG-CN) hybrid nanocomposite.

Fig. 7: Thermo gravimetric analysis of PSS functionalized MnO_2 nanorods, and N doped (FLG-CN) hybrid nanocomposite.

Fig. 8: EDS spectrum (a) and elemental mapping of N doped (FLG-CN) hybrid nanocomposite (b,c,d) are showing the distribution of C, N and O.

Fig. 9: (a) Galvanostatic charge–discharge curves of N doped (FLG-CN) hybrid nanocomposite in the voltage range of 0.01–3 V *vs.* Li/Li^+ electrode acquired at a current density of 100 mA g^{-1}. (b) Charge–discharge curves of N doped (FLG-CN) at different high current densities.

Fig. 10: (a) Galvanostatic charge–discharge curves of few layer graphene in the voltage range of 0.01–3 V *vs.* Li/Li^+ electrode acquired at a current density of 100 mA g^{-1}. (b) Charge–discharge curves of few layer graphene at different high current densities.

Fig. 11: Cyclic stability of N doped (FLG-CN) hybrid nanocomposite for the initial 500 cycles at the current density of 500 mA g^{-1} (a), and subsequent 500 cycles at the current density of 5000 mA g^{-1}.

Fig.12: Nyquist plot and the equivalent circuit for N doped (FLG-CN) and few layer graphene electrode.

Fig. 13: Schematic illustration of lithium adsorption and desorption in N doped (FLG-CN) electrode material.

Figures

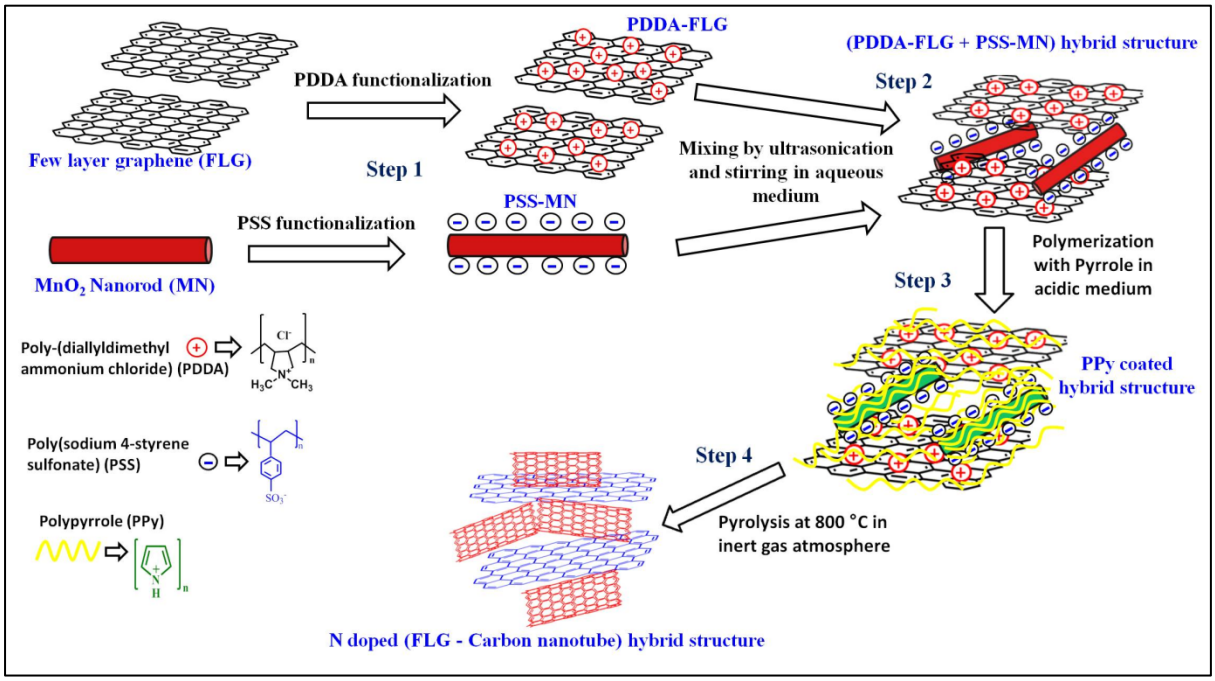

Fig. 1

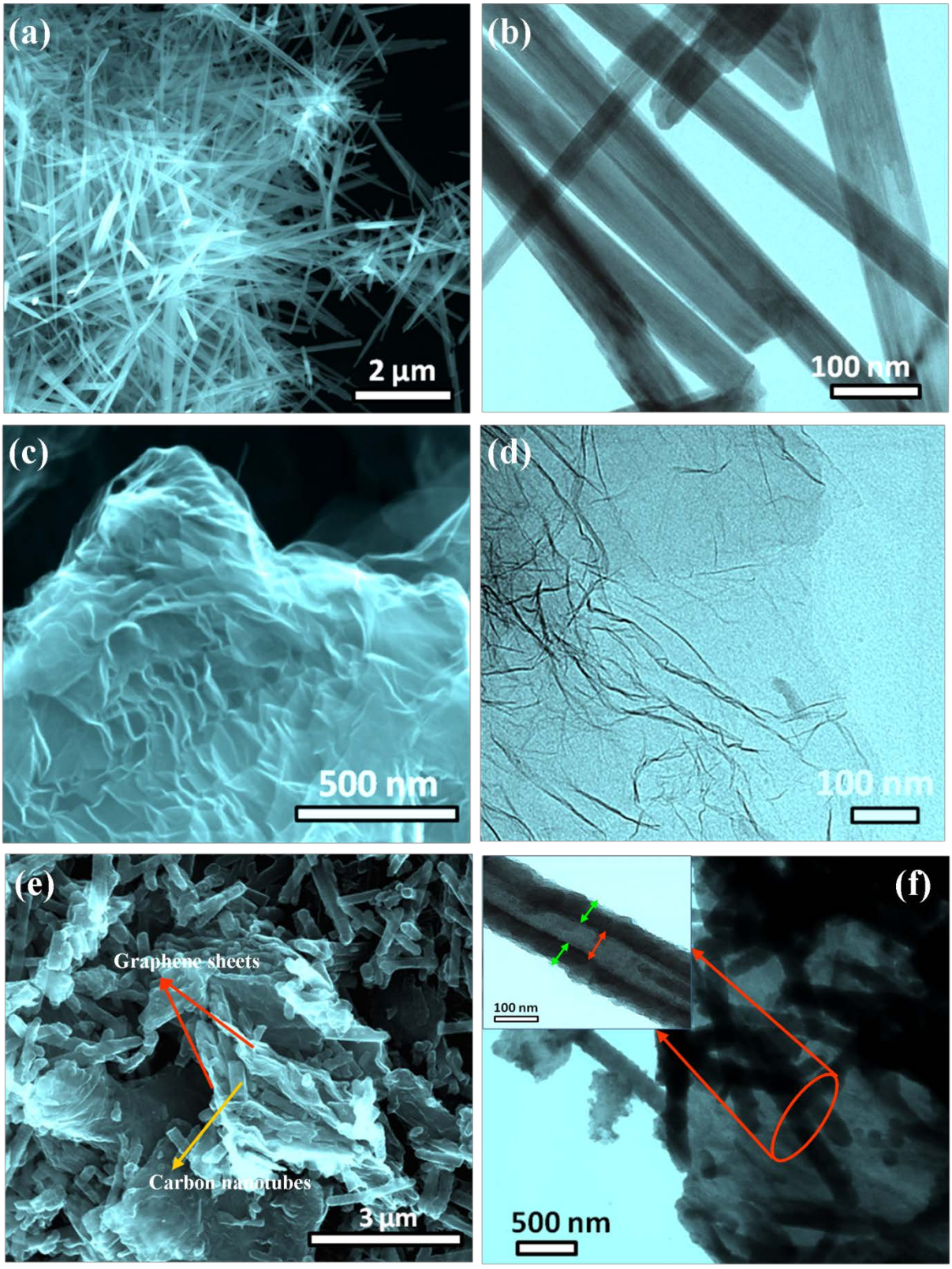
(a)
2 µm
(b)
100 nm
(c)
500 nm
(d)
100 nm
(e)
Graphene sheets
Carbon nanotubes
3 µm
(f)
100 nm
500 nm

Fig. 2

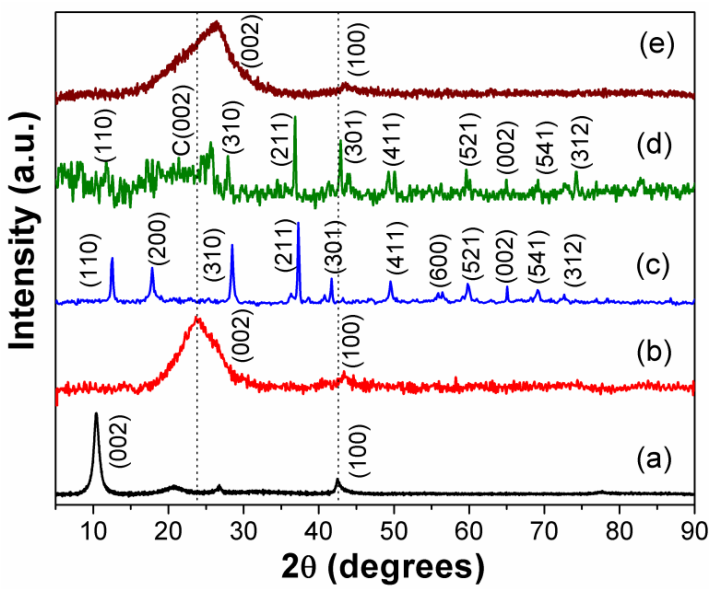
Intensity (a.u.)
2θ (degrees)
10
20
30
40
50
60
70
80
90
(e)
(d)
(c)
(b)
(a)
(002)
(100)
(110)
C(002)
(310)
(211)
(301)
(411)
(521)
(002)
(541)
(312)
(200)
(600)

Fig. 3

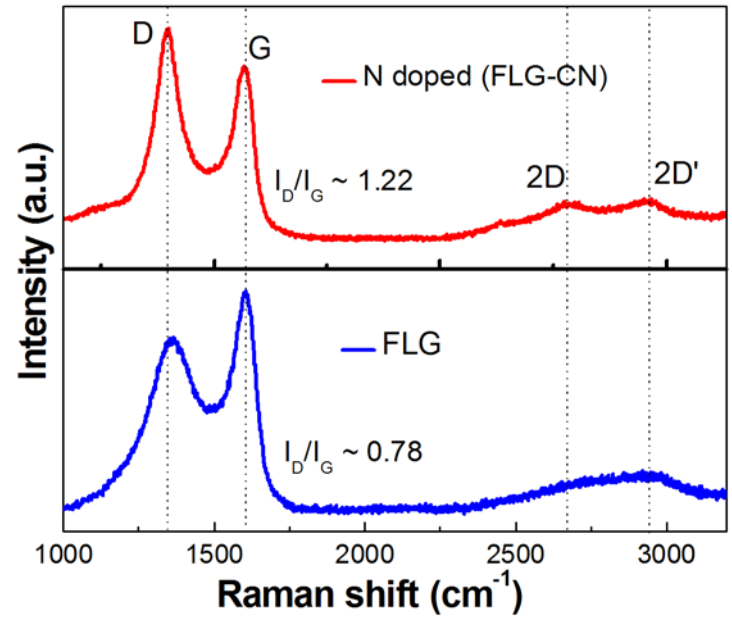
D
G
N doped (FLG-CN)
I_D/I_G ~ 1.22
2D
2D'
FLG
I_D/I_G ~ 0.78
Intensity (a.u.)
1000
1500
2000
2500
3000
Raman shift (cm^{-1})

Fig. 4

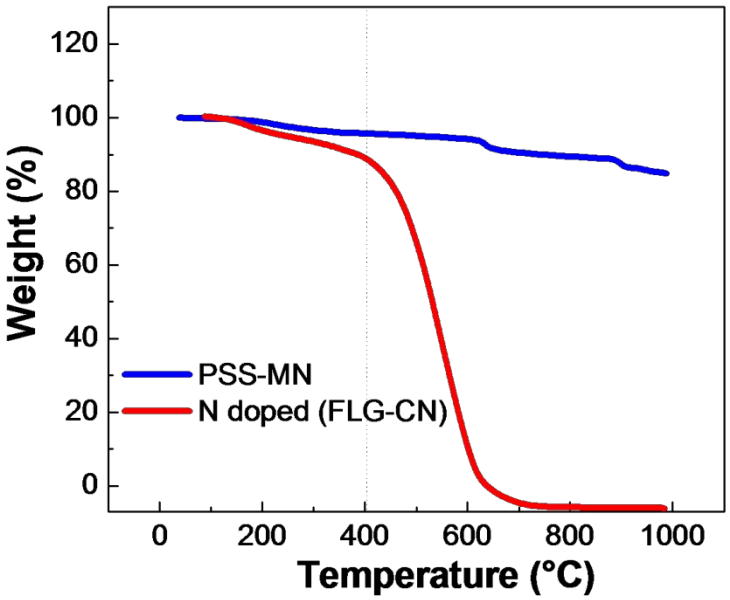
Weight (%)
120
100
80
60
40
20
0
0
200
400
600
800
1000
Temperature (°C)
PSS-MN
N doped (FLG-CN)

Fig. 5

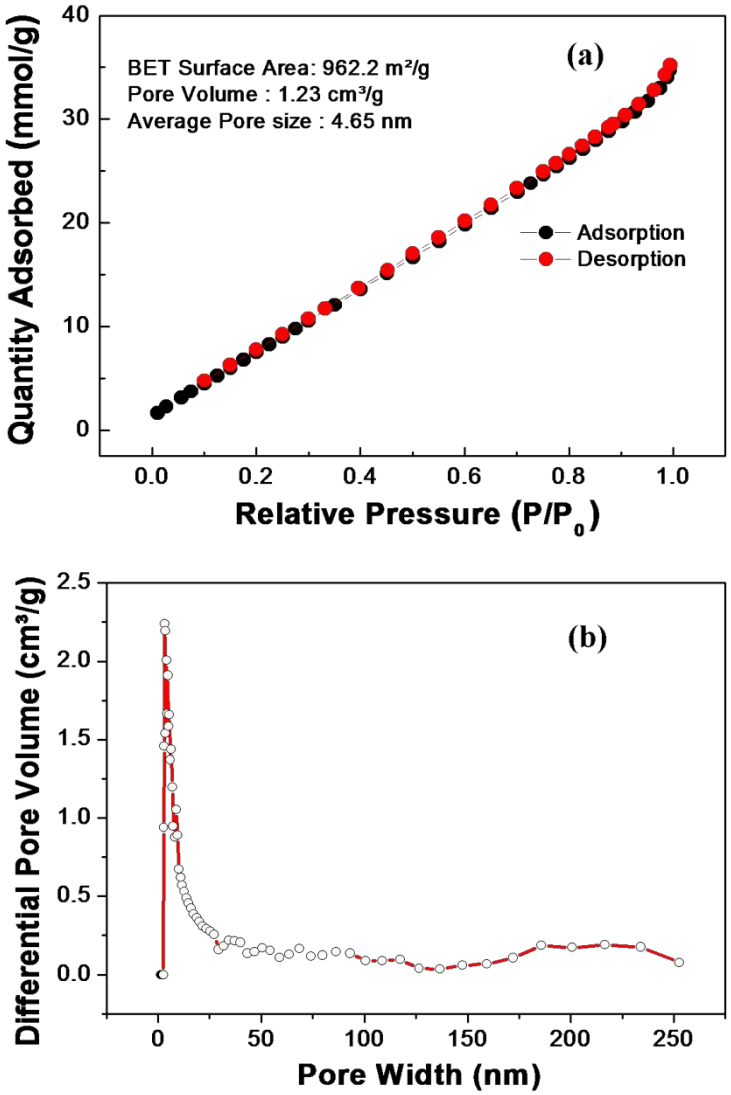
(a)
BET Surface Area: 962.2 m²/g
Pore Volume : 1.23 cm³/g
Average Pore size : 4.65 nm
Adsorption
Desorption
Quantity Adsorbed (mmol/g)
Relative Pressure (P/P0)
(b)
Differential Pore Volume (cm³/g)
Pore Width (nm)

Fig. 6

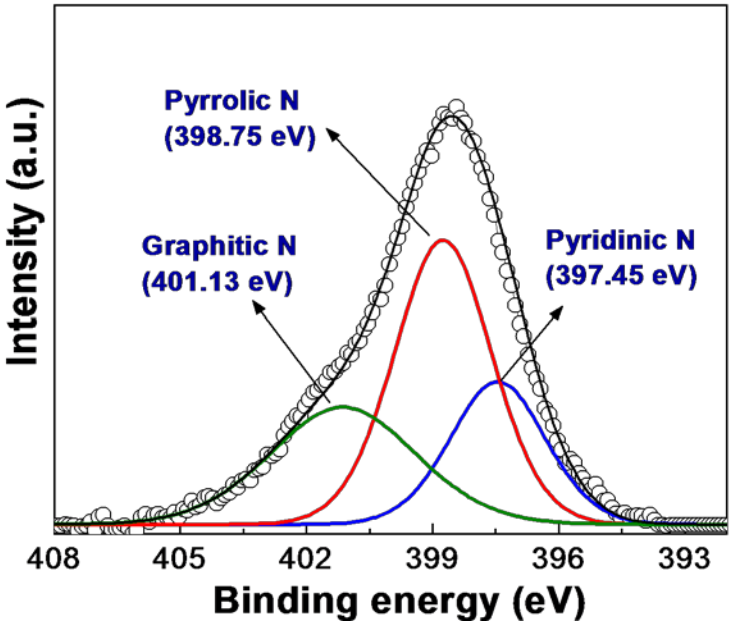
Pyrrolic N
(398.75 eV)
Graphitic N
(401.13 eV)
Pyridinic N
(397.45 eV)
Intensity (a.u.)
408
405
402
399
396
393
Binding energy (eV)

Fig. 7

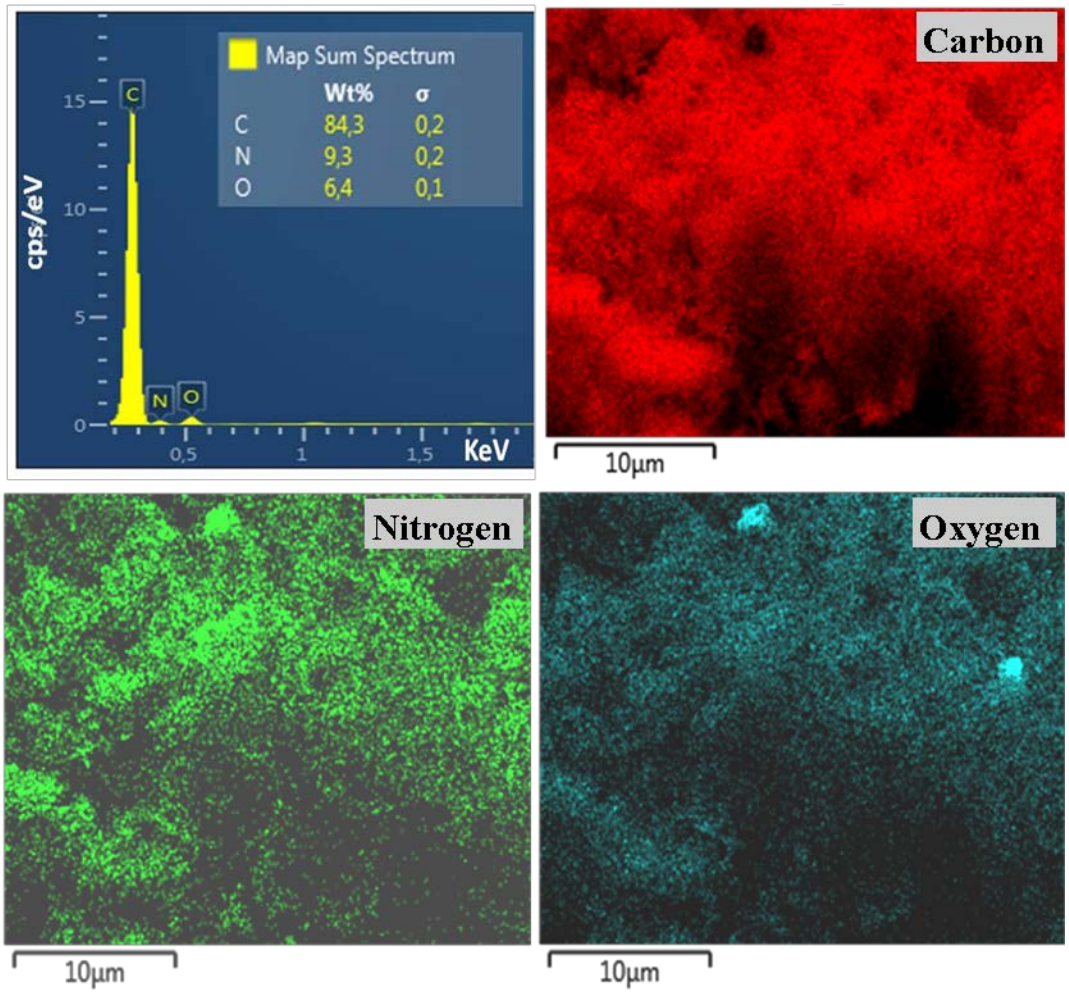
Map Sum Spectrum
Wt% σ
C 84,3 0,2
N 9,3 0,2
O 6,4 0,1
cps/eV
15
10
5
0
C
N
O
0,5
1
1,5
KeV
Carbon
10µm
Nitrogen
10µm
Oxygen
10µm

Fig. 8

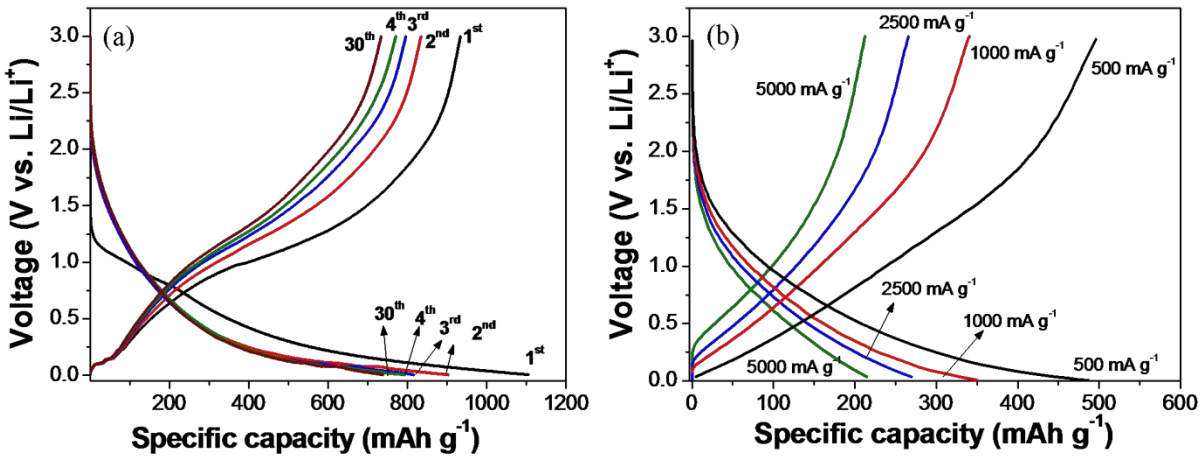
(a)
Voltage (V vs. Li/Li+)
Specific capacity (mAh g-1)
30th
4th
3rd
2nd
1st
(b)
2500 mA g-1
1000 mA g-1
500 mA g-1
5000 mA g-1

Fig. 9

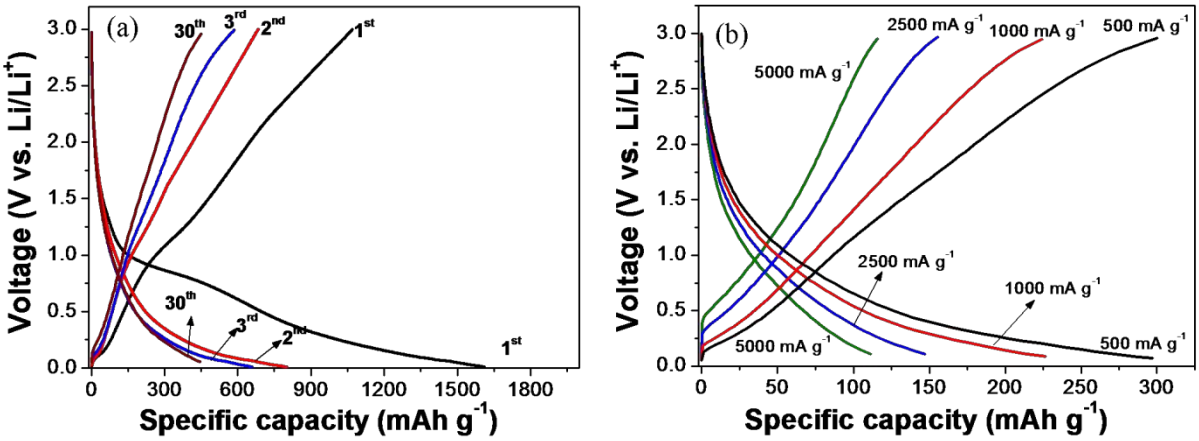
(a)
30th
3rd
2nd
1st
Voltage (V vs. Li/Li+)
Specific capacity (mAh g-1)
(b)
2500 mA g-1
1000 mA g-1
500 mA g-1
5000 mA g-1

Fig. 10

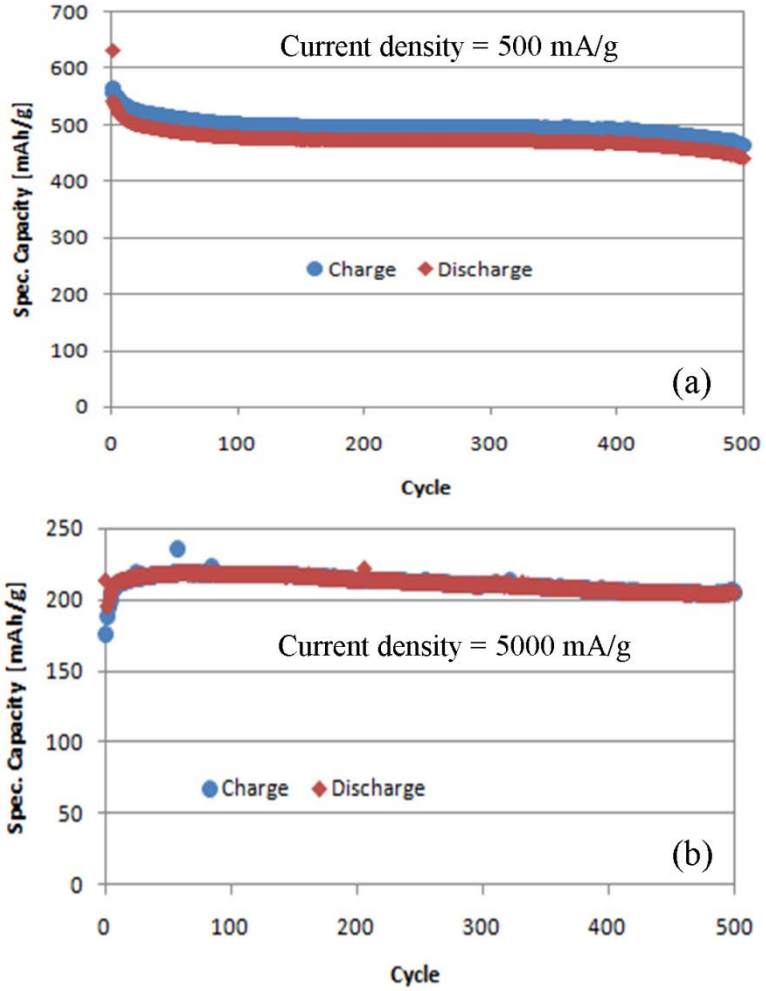
Current density = 500 mA/g
Spec. Capacity [mAh/g]
Charge
Discharge
(a)
Cycle
Current density = 5000 mA/g
Spec. Capacity [mAh/g]
Charge
Discharge
(b)
Cycle

Fig. 11

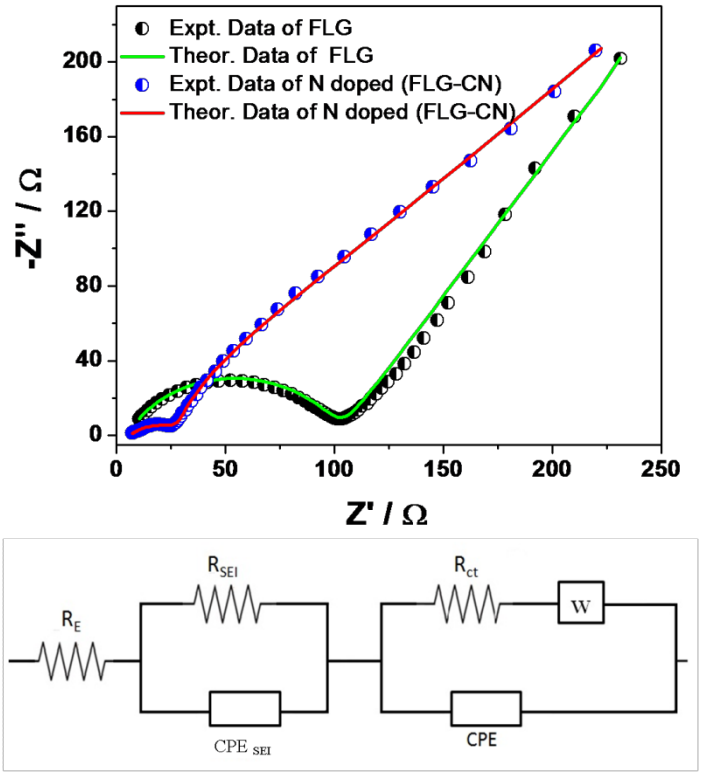
Expt. Data of FLG
Theor. Data of FLG
Expt. Data of N doped (FLG-CN)
Theor. Data of N doped (FLG-CN)
-Z'' / Ω
Z' / Ω
0
40
80
120
160
200
0
50
100
150
200
250
R_E
R_SEI
CPE_SEI
R_ct
W
CPE

Fig. 12

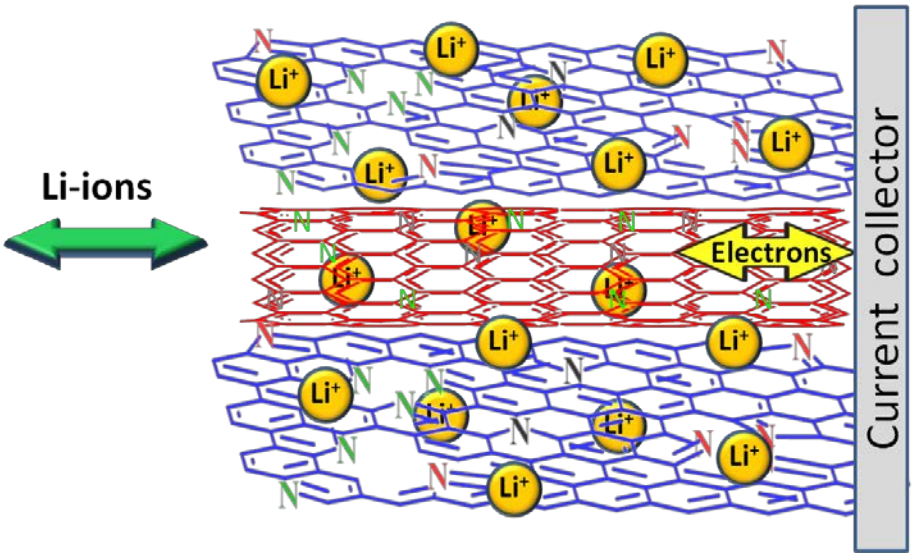

Fig. 13